ISSN 0001-4338, Izvestiya, Atmospheric and Oceanic Physics, 2017, Vol. 53, No. 6, pp. 592–602. © Pleiades Publishing, Ltd., 2017.
Original Russian Text © N.M. Gavrilov, A.V. Koval, A.I. Pogoreltsev, E.N. Savenkova, 2017, published in Izvestiya Rossiiskoi Akademii Nauk, Fizika Atmosfery i Okeana, 2017, Vol. 53, No. 6, pp. 674–685.

Numerical Simulation of Wave Interactions during Sudden Stratospheric Warming

N. M. Gavrilov[a], *, A. V. Koval[a], **, A. I. Pogoreltsev[b], and E. N. Savenkova[a]

[a] *Atmospheric Physics Department, Saint Petersburg State University, St. Petersburg, 198504 Russia*
[b] *Meteorological Forecast Department, Russian State Hydrometeorological University, 195196 Russia*
**e-mail: n.gavrilov@spbu.ru*
***e-mail: koval_spbu@mail.ru*

Received October 28, 2016; in final form, December 27, 2016

Abstract—Parameterizations of normal atmospheric modes (NAMs) and orographic gravity waves (OGWs) are implemented into the mechanistic general circulation model of the middle and upper atmosphere (MUA). Numerical experiments of sudden stratospheric warming (SSW) events are performed for climatological conditions typical for January and February using meteorological reanalysis data from the UK MET Office in the MUA model averaged over the years 1992–2011 with the easterly phase of quasi-biennial oscillation (QBO). The simulation shows that an increase in the OGW amplitudes occurs at altitudes higher than 30 km in the Northern Hemisphere after SSW. The OGW amplitudes have maximums at altitudes of about 50 km over the North American and European mountain systems before and during SSW, as well as over the Himalayas after SSW. At high latitudes of the Northern Hemisphere, significant (up to 50–70%) variations in the amplitudes of stationary planetary waves (SPWs) are observed during and after the SSW. Westward travelling NAMs have local amplitude maximums not only in the Northern Hemisphere, but also in the Southern Hemisphere, where there are waveguides for the propagation of these modes. Calculated variations of SPW and NAM amplitudes correspond to changes in the mean temperature and wind fields, as well as the Eliassen-Palm flux and atmospheric refractive index for the planetary waves, during SSW. Including OGW thermal and dynamical effects leads to an increase in amplitude (by 30–70%) of almost all SPWs before and during SSW and to a decrease (up to 20–100%) after the SSW at middle and high latitudes of the Northern Hemisphere.

Keywords: atmospheric circulation, modeling, middle and upper atmosphere, planetary waves, orographic gravity waves, parameterization, sudden stratospheric warming

DOI: 10.1134/S0001433817060044

INTRODUCTION

Sudden stratospheric warmings (SSWs) are one of the most notable manifestations of the dynamic interactions of the troposphere and the middle layers of the atmosphere. These phenomena are manifested in sharp and significant increases in temperature (up to 30–40 K) near the North Pole at altitudes of 30–50 km and in weakening or even reversal of the western polar circumpolar vortex [1, 2]. The formation of SSW can be facilitated by unstable planetary waves (PWs) propagating upward from the troposphere [3–5].

In recent years, there is growing interest in the study of SSWs [6–8]. SSW phenomena greatly affect the dynamics and energy of the upper layers of the atmosphere [9–12] and, accordingly, can impact space weather. Despite growing interest in the study of SSW, many questions related to the mechanism of SSW formation [13] and its influence on planetary and gravitational waves [14] remain open.

The transfer of kinetic energy and momentum by internal waves is a necessary condition for the interaction between dynamic processes in the lower and middle layers of the atmosphere [15, 16]. Numerical models of the temperature regime and global circulation of the middle layers of the atmosphere take into account the influx of heat and accelerations created by dissipating internal waves [17, 18]. One important source of internal atmospheric waves is the relief of the Earth's surface [19]. Numerical experiments devoted to the effect of gravitational waves on global circulation, the amplitude of tides, and their seasonal changes are described in [20–23]. The irregularity and instability of the process of appearance of gravitational waves and conditions for their propagation into the middle layers of the atmosphere generate various modes of PWs (for example, [24–26]). Gavrilov et al. [27] included parameterization of the dynamic and thermal effects of OGWs in the mechanistic numerical circulation model of the middle and upper atmosphere (MUA). It was shown that OGWs can significantly affect global

Table 1. Time intervals used to estimate the parameters of PWs before, during, and after SSW simulated with and without OGS parameterization in the MUA model

	Before SSW	During SSW	After SSW
With OGW	January 6–16	January 19–29	February 4–14
Without OGW	January 18–28	February 8–18	February 20–March 2

circulation in the middle and upper layers of the atmosphere. In [28], the authors simulated changes in the amplitudes of PW caused by OGWs.

In this study, numerical experiments were carried out to investigate the interaction of PWs and OGWs in the middle atmosphere during SSW. We included the parameterization of normal atmospheric modes (NAMs) into the MUA model (MUAM) and analyzed changes in amplitudes of stationary planetary waves (SPWs) and NAMs propagating to the west during 11-day time intervals before, during, and after the SSW with and without the parameterization of OGW effects for climatological conditions typical for January–February.

1. MODEL OF GLOBAL CIRCULATION OF MUA AND PARAMETRIZATION OF OGW

In order to study the OGW effect on characteristics of PW during SSW events, we conducted a numerical experiment using the MUAM described by Pogoreltsev [29]. In this study, we used the meteorological parameter distribution fields averaged for January–February for all years with the easterly phases of QBOs during 1992–2011 according to the list of "easterly" and "westerly" phases [30, 31]. The MUAM can reproduce SPWs and propagating NAMs. At the lower boundary, the amplitudes of SPW are estimated based on data on geopotential altitudes in the lower atmosphere taken from the above meteorological data of the UK Met Office.

For the parameterization of NAM sources, the authors of [32] added additional terms to the thermal balance equation in the MUAM, which contain a series of sinusoidal components with zonal wave numbers $m = 1$ and $m = 2$ and periods corresponding to the analyzed NAMs. The NAM periods correspond to the resonant response of the lower atmosphere to wave oscillations [32]. The version of MUAM used includes westward NAMs (1,1), (1,2), (2,1), and (2,2) according to the classification [33]. They have resonant periods of 120, 220, 90, and 170 h, respectively. These sources provide amplitudes of simulated NAMs comparable to those observed in the stratosphere [34]. The parameterization of the dynamic and thermal effects of OGW with the observed frequencies $\sigma = 0$ was described in [35].

Numerical experiments with the MUAM were carried out for two cases: with and without OGW parameterization. The modes of SPW with zonal wave numbers $m = 1$–4 and NAM of the western direction with $m = 1$ and $m = 2$, having periods of 5, 10 and 4, 7 days, respectively, are analyzed, as are their changes due to the OGW impact.

2. EXPERIMENTAL RESULTS

The characteristics of PWs caused by the impact of orographic waves are simulated for three 11-day intervals before, during, and after SSW in the middle atmosphere.

2.1. Changes in Zonal Mean Characteristics

Calculations with the MUAM for climatically averaged background meteorological fields (see Chapter 1) show a sharp increase in simulated temperature by 15–20 K near the North Pole with a simultaneous turn of the mean zonal velocity at a latitude of 62° N at altitudes of 25–30 km at the end of January, which is typical for the major SSW. According to the UK Met Office, similar warming was observed in January–February 2001. A simulation showed that amplitudes of PWs with a zonal wave number $m = 1$ at an altitude above 30 km increases during SSW and decreases after the completion of the SSW. The time intervals corresponding to the condition before, during, and after the model average climate SSW are given in Table 1. The table shows that including OGW parameterization leads to an earlier (by 20 days) development of SSW.

Figure 1 shows the altitude–latitudinal distributions of zonal wind, deviations of temperature from its 2-month averages, and amplitudes of OGWs for 11-day intervals before, during and after the VSP, calculated according to the MUAM and averaged over longitude. The structure of zonal circulation, shown in Fig. 1a, corresponds to empirical models [36, 37]. The middle panel in Fig. 1a shows a significant attenuation of zonal mean jet stream in the high-latitude northern stratospheric mesosphere during SSW (see the right panel of Fig. 1a). This jet stream increases again after SSW, but remains weaker than before the SSW (see the left panel of Fig. 1a). This may be due to the seasonal rearrangement of zonal circulation at the end of winter.

The middle panel in Fig. 1b shows an increase in temperature near the North Pole during SSW, which reaches 15 K at altitudes of 30–50 km. Above 60 km in Fig. 1b, we can see a decrease in the subpolar temperature to –10 K during the SSW. The right panel of Fig. 1c shows an increase in the amplitude of OGW at altitudes above 30 km after the SSW. An analysis of the

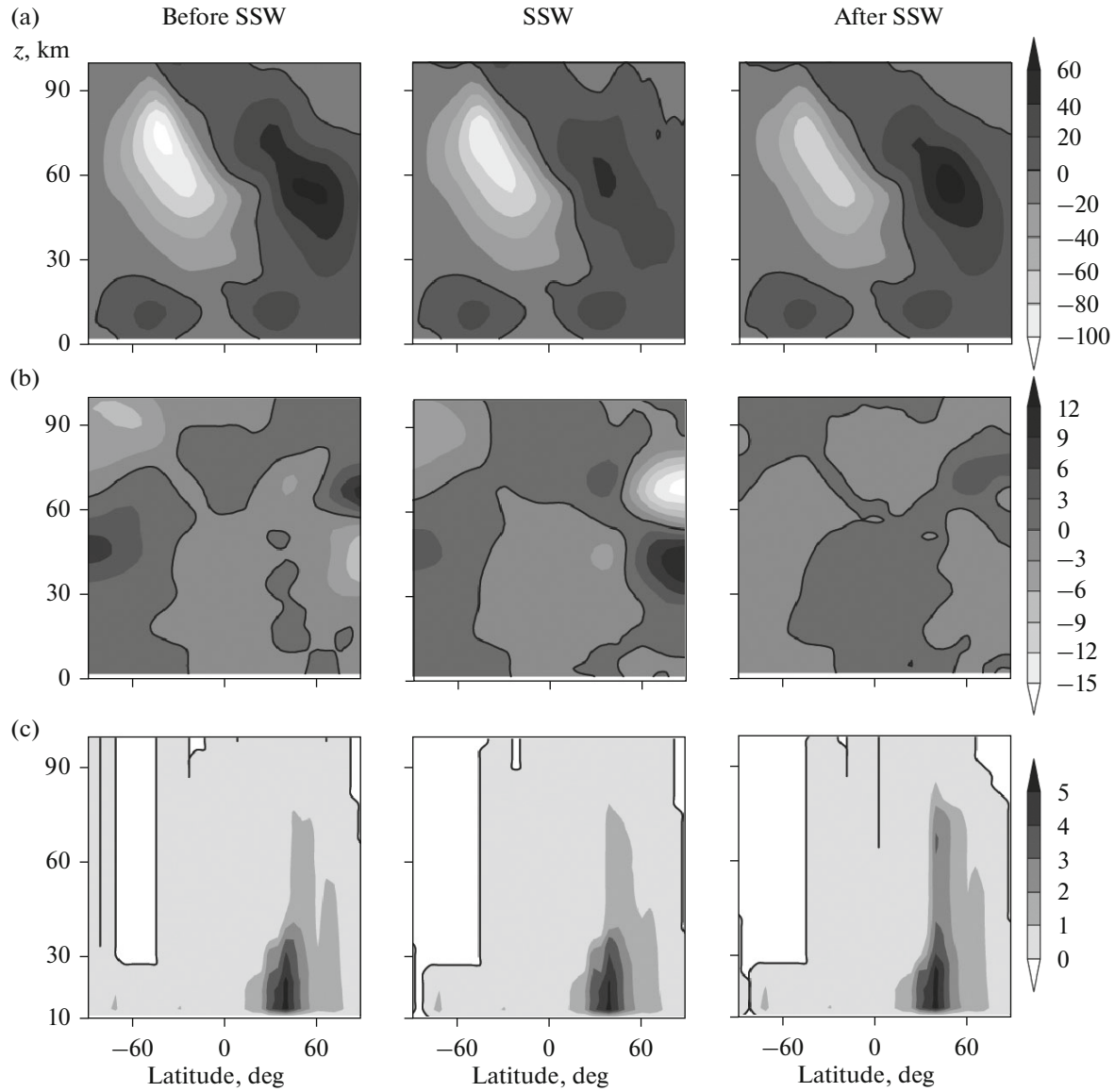

Fig. 1. Latitude–altitudinal distributions of zonal mean wind (m/s) (a), deviations of the mean-zonal temperature from the 2-monthly mean (K) (b), and OGV velocity amplitude (m/s) (c) calculated in the MUA model and averaged over 11-day time intervals (left panels) before, (middle panels) during, and (right panels) after SSW (see Table 1).

calculated horizontal distributions of the zonal wind shows that the areas of maximum values of the average easterly wind are located at midlatitudes over North America and Europe before and during SSW. After SSW, the regions of the maximum values of zonal winds are shifted to the east. Therefore, at altitudes greater than 50 km, OGWs over the mountain systems of North America and Europe have larger amplitudes before and during SSW, while after SSW, OGWs over the Himalayas become stronger.

2.2 Amplitudes of Planetary Waves

To analyze changes in PWs during SSW, the meteorological fields simulated with the MUAM that included OGW parameterization are expanded into the Fourier series for the longitude. The parameters of stationary planetary waves with zonal numbers $m = 1–4$ (designated below as SPW1–SPW4) and normal atmospheric modes propagating to the west (see Chapter 1) have been determined as suggested in [38].

Figure 2 shows the amplitudes of variations of the geopotential altitude SPW1–SPW4 for the time intervals from Table 1. It can be seen that the amplitudes of SPWs are larger in the Northern (winter) Hemisphere in January, where zonal circulation has an easterly direction at all altitudes (see Fig. 1a) and creates waveguides for the propagation of planetary waves (see below). The middle panel in Fig. 2a shows an increase in the amplitude of SPW1 at an altitude

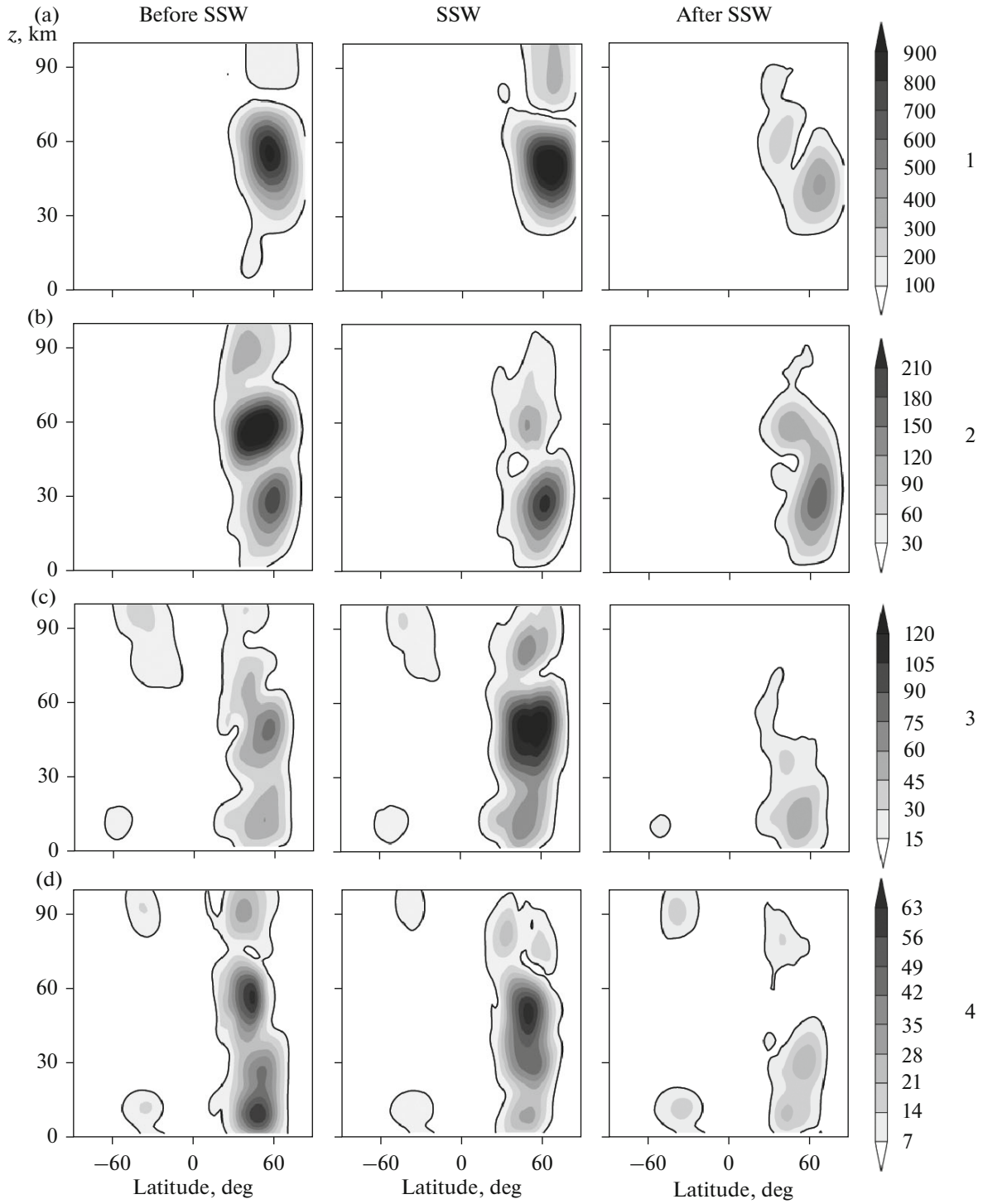

Fig. 2. Amplitudes of the geopotential variations (gpm) caused by SPWs with zonal wave numbers $m = 1, 2, 3, 4$ (a, b, c, d), (left panels) before, (middle panels) during, and (right panels) after SSW (see Table 1).

of 30–40 km in the region of the North Pole during SSW. The interaction of SPW1 with the average jet stream, shown in Fig. 2a, can change the direction of the wind at high latitudes from west to east.

Figure 2b shows that the amplitude peak of the SPW2 with $m = 2$ increases before SSW and decreases during and after it at altitudes of 50–70 km in the Northern Hemisphere. The maximum amplitude of SPW2 at altitudes of 20–40 km in Fig. 2b amplifies during SSW and can contribute to the formation of temperature and wind structures with two maxima and minima along the latitude circle (these structures

are revealed in the analysis of horizontal distributions of corresponding simulated fields during SSW). The relative changes in the amplitudes of SPW1 and SPW2 during SSW can be caused by nonlinear interactions between modes of PW and changes in their phases. Figures 2c and 2d show an increase in the amplitudes of SPW3 and SPW4 in the Northern Hemisphere during SSW. The right panels of Fig. 2 show a general decrease in the amplitudes of all PWs after the completion of SSW, which can be caused by transformations of background winds and temperature fields that affect the propagation conditions of SSW.

Figure 3 depicts the amplitudes of geopotential variations created by NAM modes with different periods, which propagate to the west. The features of Fig. 3 are the maximums of the NAM amplitudes not only in the Northern, but also in the Southern Hemisphere, where the NAMs propagating to the west may have waveguides for their propagation (see Chapter 2.3). In the middle and high latitudes of the Northern Hemisphere in Fig. 3, the amplitudes of 4- and 5-day NAMs decrease and the amplitudes of 7- and 10-day NAMs increase during SSW. The amplitude of NAMs increases in the Southern Hemisphere at altitudes higher than 40 km after the end of SSW (see the right panels of Fig. 3). This may be a result of seasonal restructuring of global atmospheric circulation shown in Fig. 1a, which makes the average atmosphere of the Southern Hemisphere more "transparent" for the NAMs spreading to the west.

2.3 REFRACTIVE INDICES OF PW AND THE ELIASSEN-PALM FLUXES

Areas of the atmosphere in which the background temperature and wind create conditions for the propagation of PW are considered as waveguides. Dickinson [39] and Matsuno [40] introduced the refractive index of the atmosphere for PW and showed that planetary waves propagate best in the regions with positive values of this index. To study the structure of PW waveguides during SSW, the formulas for calculating the square of mean zonal quasi-geostrophic refractive index n_m^2 for wave modes with a zonal wave number m were used [15, 41, 42]. The theory of planetary waves suggests that waves can propagate upward in the atmospheric regions, where $n_m^2 > 0$, or fade in regions where $n_m^2 < 0$. Thus, the waveguides of atmospheric PWs are limited to regions where n_m^2 changes sign. These surfaces are located near critical PW levels.

Another important characteristic of PWs is a vector of the Eliassen-Palm flux $F_m = (F_m^{(\varphi)}, F_m^{(z)})$ (EP flux). Estimates of this flux in this study are performed by standard formulas (see [15, 41]). The divergence of the EP flux determines the acceleration of the mean zonal stream created by the PW.

The latitude–altitude distributions of positive n_m^2 for SPW1–4 were calculated. More favorable conditions for the spread of SPWs exist in midlatitudes of the Northern Hemisphere, where the EP fluxes are directed up at low altitudes and turn to the equator in the stratosphere. This is consistent with existing studies of EP fluxes (e.g. [30, 42, 43]). The analysis shows that the EP fluxes in the middle atmosphere are maximal for SPW1. An increase in m leads to a decrease in the magnitude of the EP fluxes.

We performed an analysis of simulated increments of the EP flux vectors and n_m^2 for SPW during and after SSW relative to their state before warming. The most significant increments in the refractive index were found at altitudes of 30–70 km and latitudes of 20–70° N. They correspond to changes in the zonal mean wind in Fig. 1a. For SPW1 at latitudes above 50° N, the vectors of increments of the EP fluxes during VSP have the same directions as the EP fluxes at altitudes of 30–50 km before the VSP; they have an opposite direction at altitudes of 30–90 km. The increase and decrease of the EP fluxes corresponds to the increase and decrease of SPW1 amplitudes on the middle panel of Fig. 2a. The opposite direction of the EP vectors after warming corresponds to a decrease in the amplitude of SPW1 on the right panel of Fig. 2a. A similar dependence exists for the SSW with $m > 1$. The direction of the increment vectors of the SPW2 EP fluxes during and after the SSW is mainly opposite the directions of these fluxes before the warming and corresponds to the decreases in SPW2 amplitudes on the middle and right panel of Fig. 2b at high latitudes of the Northern Hemisphere. The amplitudes of SPW3 and SPW4 in the Northern Hemisphere are larger on the middle and smaller on the right panels of Figs. 2c and 2e than amplitudes on the left panels.

The NAMs propagating to the west may have regions with $n_m^2 > 0$ in the areas of the eastern winds of the Southern (summer) Hemisphere. Analysis of the EP flux vectors shows that the NAMs spreading to the west are generated mainly in midlatitudes of the Northern Hemisphere, from where they propagate to the regions of the Southern Hemisphere along waveguides with $n_m^2 > 0$. Thus, NAMs may have significant amplitudes in both hemispheres. The largest amplitudes in the Southern Hemisphere on the left panels of Fig. 3 have NAMs with periods of 4 and 5 days with the greatest horizontal phase velocities $c = -61$ m/s and $c = -95$ m/s at the equator, respectively. Thus, the westerly spreading NAMs can participate in dynamic connections between both hemispheres of the middle atmosphere. Before SSW, the vertical components of the EP flux are usually directed upward in the middle atmosphere of the middle and high northern latitudes. According to the theory, this corresponds to the heat fluxes created by SPWs and NAMs directed to the north and to probable heating of the middle atmo-

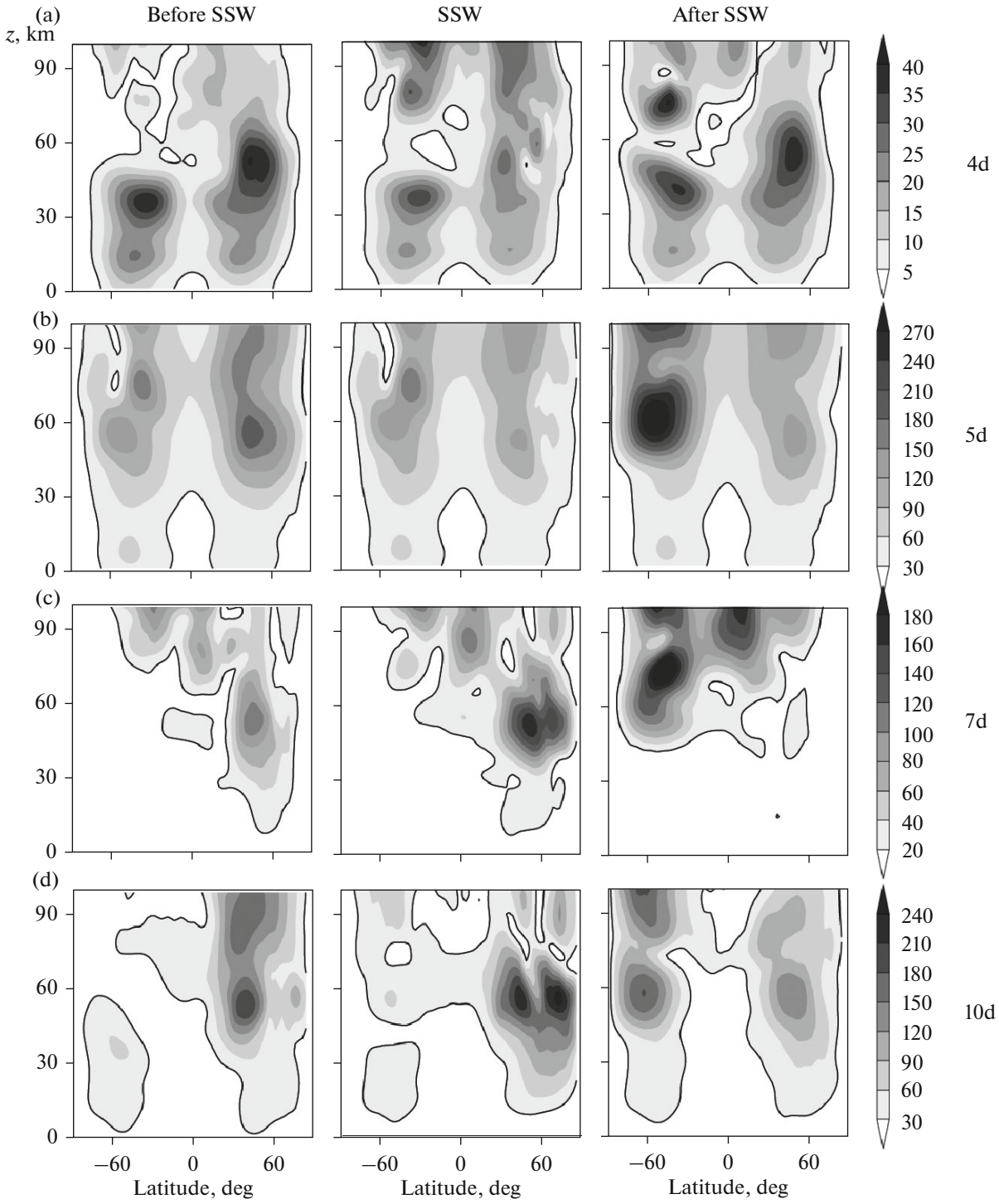

Fig. 3. Amplitudes of the geopotential variations (gpm) caused by propagating westward NAMs with $\tau = 4$ days, $m = 2$ (a); $\tau = 5$ days, $m = 1$ (b); $\tau = 7$ days, $m = 2$ (c); $\tau = 10$ days, $m = 1$ (d), (left panels) before, (middle panels) during, and (right panels) after SSW (see Table 1).

sphere near the North Pole, which can contribute to the development of SSW during the winter season.

The vectors of the increments of the EP fluxes during and after SSW can have a direction both coinciding with and opposite to the direction of the corresponding fluxes before the warming. Thus, the changes in the amplitudes of the NAMs propagating westward in Fig. 3 are positive or negative, depending on the increase or decrease of n_m^2 and magnitude of the EP fluxes. Therefore, changes in the conditions of

NAM propagation can affect the temperature regime in the middle Arctic atmosphere.

One interesting feature of the right panels of Fig. 3 is an increase in the amplitude of the NAMs in the Southern Hemisphere after SSW. The analysis shows significant changes in n_m^2 values in the regions with the maximum amplitude of NAMs spreading westward in the Southern Hemisphere. These changes may be related to both the SSW and the seasonal transformations of zonal mean wind fields and temperature in the Southern Hemisphere. Thus, the changes in the amplitudes of SPWs and NAMs in Figs. 2–3 can be associated with changes in the refractive index of the atmosphere for PVs due to changes in the background mean temperature and wind, as well as changes in EP fluxes before, during, and after SSW.

2.4. EFFECT OF STATIONARY OROGRAPHIC GRAVITATIONAL WAVES

The above-described numerical experiments with the MUA model were carried out using parameterization of the dynamic and thermal effects of OGWs (see Chapter 1). According to Table 1, the inclusion of OGW parameterization leads to an earlier (approximately by 20 days) development of the SSW. In order to compare the results of experiments with and without OGW parameterization, we calculated increments in PW amplitudes with included OGW parameterization and averaged over the time intervals shown in Table 1 before, during, and after the SSW. Positive or negative increments correspond to an increase or decrease in the amplitude of the PW when OGW parameterization is switched on.

Figure 4 shows increments in amplitudes of variations of geopotential altitudes for SPW1–SPW4. The overall increase (up to 70%) in the amplitudes of the most SPWs can be seen on the left and middle panels of Fig. 4 for the middle and high latitudes of the Northern Hemisphere before and during SSW. The increments in SPW3 amplitudes on the left panels of Fig. 4 are less significant. As is shown in Fig. 4, for SPW1 occurring before SSW at altitudes below 50 km and for SPW2 that takes place during SSW at altitudes of 30–60 km with the inclusion of OGW parameterization, the amplitudes decrease to 50%. After the SSW, in the middle and high latitudes of the Northern Hemisphere, on the right panels of Fig. 4, the negative increments in the SPW amplitudes (decrease down to 50%) prevail when OGW parameterization is included. The right panel in Fig. 4b shows a positive increment in the amplitude of SPW2 at altitudes below 60 km after SSW. The features of the horizontal distribution of OGW generation, described in Chapter 3.1, can change the distribution of wave accelerations in the middle atmosphere and differently affect SPW amplitudes in different time phases of SSW.

To check the statistical reliability of nonzero values of the increments in SPW amplitudes, the paired statistical Student's *t*-test was used in Fig. 4a [44]. The increments shown in Fig. 4 for each range of altitude and latitude and each 11-day interval listed in Table 1 are obtained by averaging the differences of 4224 pairs of SPW amplitudes at 64 nodes of the longitudinal grid and 66 times (4-h output of the results). A paired Student's *t*-test has shown the statistical reliability of nonzero increments of SPW amplitudes above 95% if their absolute values in Fig. 4 exceed 6–9 gpm.

For a better understanding of the mechanism of the OGW effect, we calculated the differences in the EP fluxes and refractive indices of the atmosphere for PWs (see Chapter 2.3). The analysis has shown that—in accordance with the PW theory—the positive increments in SPW amplitudes in Fig. 4 correspond to decreases in n_m^2 and increases in the moduli of the EP flux vectors for the respective SPW modes.

Figure 5 shows the increments of the amplitudes of NAMs propagating to the west, which are caused by the inclusion of OGW parametrization in the MUAM. On the left panel of Fig. 5a, the OGW impact increases the amplitude of the 4-day NAM before the SSW at altitudes of 30–70 km and latitudes of 30–60° N. This corresponds to a significant increase in the south-directed EP fluxes and their propagation into waveguides (existing in the Southern Hemisphere) for westerly propagating NAMs (see Chapter 2.3). The divergence of these fluxes formed before SSW leads to negative increments in the amplitude of 4-day NAMs at altitudes above 50 km in the middle and high latitudes of the Southern Hemisphere during warming (middle panel of Fig. 5a). This decrease in the amplitude of NAM corresponds to significant changes of n_m^2 and changes in the direction of the EP fluxes that unfold in the northern direction and may have an additional dynamic effect on the amplitudes of the NAM in the Northern Hemisphere after SSW (right panel of Fig. 5a). For other westerly propagating NAMs in Fig. 5, the behavior pattern of the EP fluxes and n_m^2 is similar to the described one, with some features for each particular mode. Thus, trans-equatorial EP fluxes can play an important role in dynamic interactions at different stages of SSW. In this study, only one set of average climatological data is used, which corresponds to a typical event of major SSW. The impact of OGV may both increase and decrease the amplitudes of different SPW and NAM modes in different ways in each individual SSW case. Therefore, simple averaging over the SSW ensemble can lead to the compensation of these changes and a false underestimation of the OGW effects that can be significant in each specific case. Thus, it is important to study features of the OGV effects for each SSW case before performing their statistical analysis.

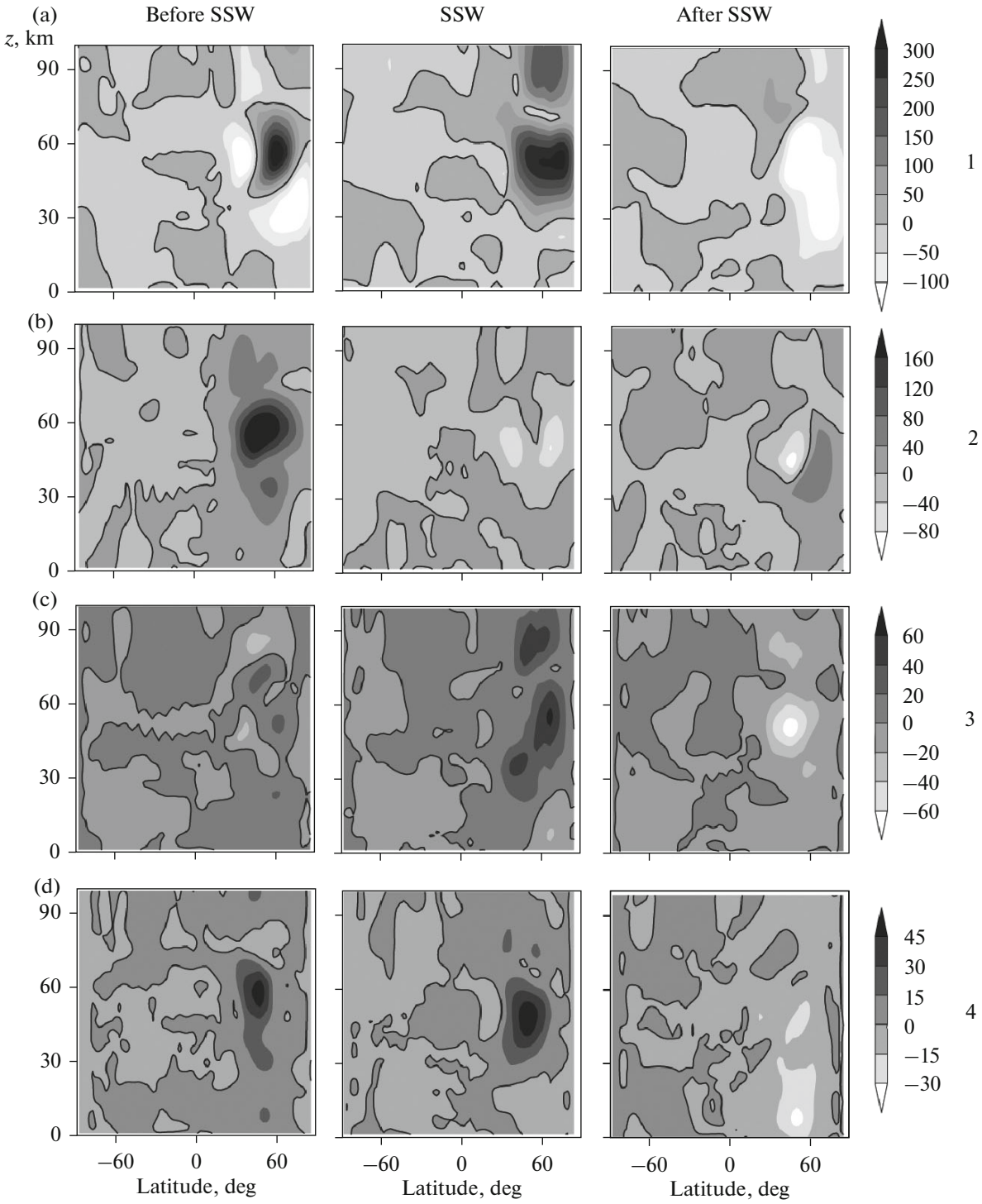

Fig. 4. Differences in the amplitudes of SPW with $m = 1, 2, 3, 4$ (a, b, c, d) in the geopotential fields caused by the dynamic and thermal impact of OGW (left panels) before, (middle panels) during, and (right panels) after SSW (see Table 1). Thick lines correspond to zero values.

3. CONCLUSIONS

The MUA model of general atmospheric circulation with included parameterizations of NAMs and OGW was used for numerical experiments using the averaged data of meteorological reanalysis of the UK Met Office, which is typical for January–February for the years with easterly phase of QBO from the period of 1992–2011. The changes in the amplitudes of stationary PWs and westerly propagating NAMs are ana-

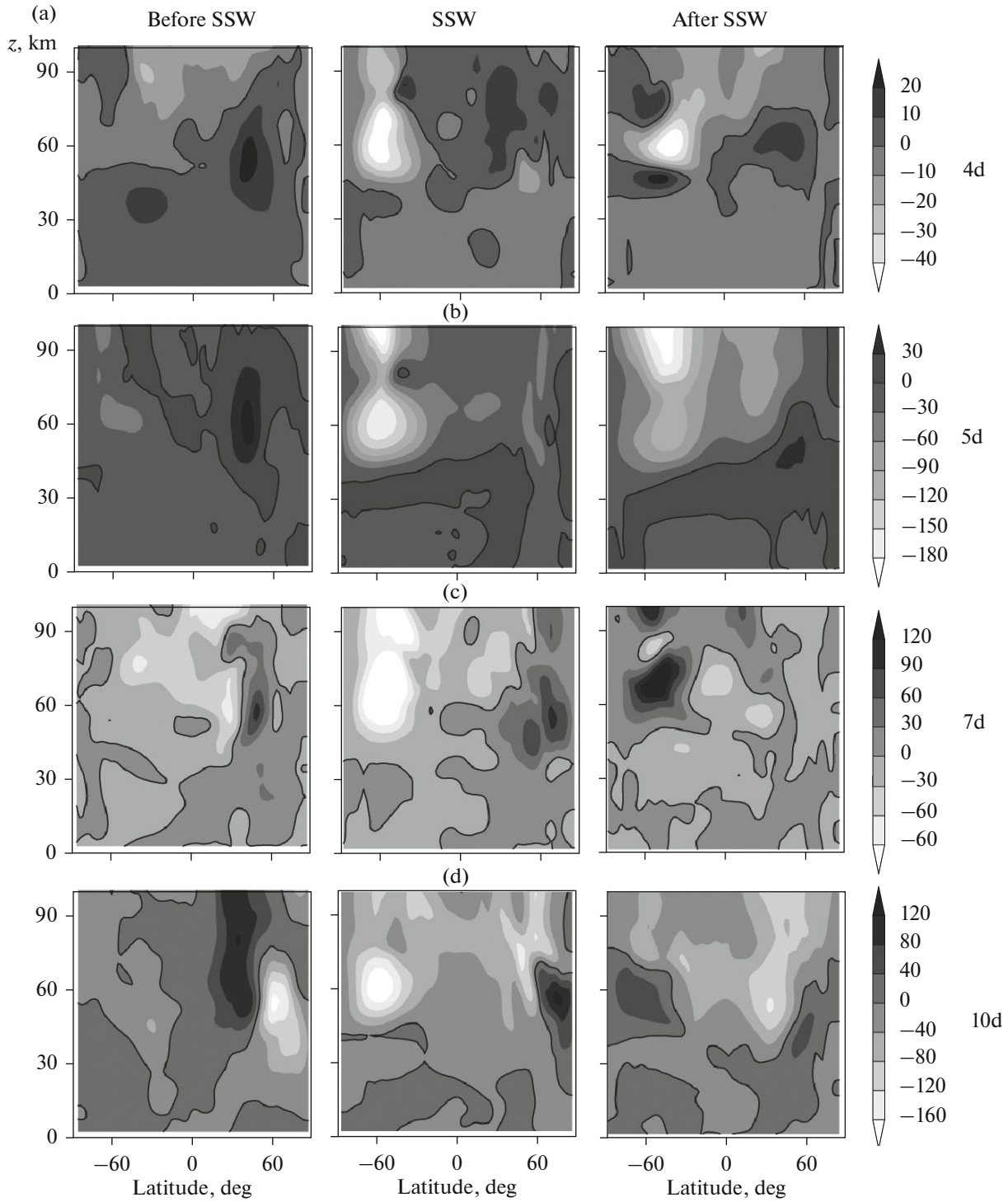

Fig. 5. The same as in Fig. 4, but for the NAMs propagating to the west with $\tau = 4$ days, $m = 2$ (a); $\tau = 5$ days, $m = 1$ (b); $\tau = 7$ days, $m = 2$ (c); and $\tau = 10$ days, $m = 1$ (d).

lyzed for time intervals before, during, and after the "climatically average" SSW phenomenon, with and without parameterization of the dynamic and thermal OGW effects.

The experiments have shown that, during the SSWs, at high latitudes of the Northern Hemisphere, the amplitudes of the SPWs with zonal wave number $m = 1, 3, 4$ increase and the amplitudes with $m = 2$ decrease. After the SSW, the amplitudes of all SPW modes decrease by 50–70% when compared to the amplitudes before the SSW. Amplitudes of westerly propagating NAMs have maxima not only in the

Northern, but also in the Southern Hemisphere due to the existence of waveguides for their propagation. In the middle and high latitudes of the Northern Hemisphere, the amplitudes of 4- and 5-day NAMs decrease, and the amplitudes of 7- and 10-day NAM increase during SSW when compared to the corresponding amplitudes before and after SSW (see Fig. 3). At altitudes of more than 40 km in the Southern Hemisphere after SSW, the amplitudes of westerly propagating NAMs increase. The calculated oscillations in the amplitudes of SPW and NAM correspond to changes in the mean temperature, wind, EP flux, and the refractive index of the atmosphere for PVs in the time intervals before, during, and after SSW.

The inclusion of parameterization of the dynamic and thermal OGW effects into the MUA model leads to an increase in the amplitudes (by 30–70%) of practically all SPW modes before and during SSW and causes their decrease (by 20–100%) after the completion of SSW at the middle and high latitudes of the Northern Hemisphere (see Fig. 4). Increases in the SPW amplitudes correspond to a decrease in n_m^2 and growth of the moduli of corresponding EP fluxes under the impact of OGVs. The NAM amplitudes grow (by 50–80%) at altitudes above 40 km under the OGW impact before SSW at medium and high northern latitudes; they decrease at midlatitudes of the Northern and Southern hemispheres during SSW and are characterized by multidirectional increments after SSW. Amplitudes of westward NAMs in the Southern Hemisphere are decreasing during SSW, which may be caused by the divergence of the southward EP fluxes that are amplified under the impact of OGWs before SSW, which propagate to the Southern Hemisphere.

This study of SPW and NAM characteristics and their changes due to the inclusion of OGW during sudden stratospheric warming was carried out only for climatological conditions typical for the eastern phase of QBOs. Earlier, the authors studied the impact of changes in the QBO phase and the effect of OGWs on planetary waves in the middle atmosphere without taking into account SSW [41]. It was shown that a change in the phase of QBOs may contribute to the change in the amplitude of SPW to ±30–90% in the middle and high latitudes of the middle atmosphere. Changes in the amplitudes of NAMs propagating westward can vary (up to 50–90%) at different altitudes and latitudes of the Northern Hemisphere due to the effects of OGWs. These changes are consistent with the distributions of the EP flux and refractive index in different phases of QBOs. To study the influence of the OGWs on planetary waves during the western phase of the QBO during SSW, additional studies are required.

ACKNOWLEDGMENTS

This work was supported by the Russian Foundation for Basic Research (project no. 16-35-60013 mol_a_dk).

REFERENCES

1. R. M. McInturff, *Stratospheric Warmings: Synoptic, Dynamic and General Circulation Aspects*, Ed. by M. McInturff (NASA, Washington, D.C., 1978).
2. M. E. McIntyre, "How well do we understand the dynamics of stratospheric warmings," J. Meteorol. Soc. Jpn., **60**, 37–64 (1982).
3. R. Quiroz, "The stratospheric evolution of sudden warmings in 1969–74 determined from measured infrared radiation fields," J. Atmos. Sci. **32**, 211–224 (1975). doi 10.1175/1520-0469(1975)032<0211:TSEOSW>2.0.CO;2
4. K. Labitzke, "Interannual variability of the winter stratosphere in the northern hemisphere," Mon. Weather Rev., **105**, 762–770 (1977). doi 10.1175/1520-0493(1977)105<0762:IVOTWS>2.0.CO;2
5. M. Schoeberl, "Stratospheric warmings—observations and theory," Rev. Geophys. **16**, 521–538 (1978). doi 10.1029/RG016i004p00521
6. M. P. Baldwin, L. J. Gray, and T. J. Dunkerton, "The quasi-biennial oscillation," Rev. Geophys. **39** (2), 179–229 (2001).
7. M. P. Baldwin, M. Dameris, and T. G. Shepherd, "How will the stratosphere affect climate change?," Science **316**, 1576–1577 (2007).
8. L. Sun and W. A. Robinson, "Downward influence of stratospheric final warming events in an idealized model," Geophys. Res. Lett. **36**, L03819 (2009). doi 10.1029/2008GL036624
9. D. E. Siskind, S. D. Eckermann, J. P. McCormack, L. Coy, K. W. Hoppel, and N. L. Baker, "Case studies of the mesospheric response to recent minor, major and extended stratospheric warmings," J. Geophys. Res. **115**, D00N03 (2010). doi 10.1029/2010JD014114
10. J. Kurihara, Y. Ogawa, S. Oyama, S. Nozawa, M. Tsutsumi, C. M. Hall, Y. Tomikawa, and R. Fujii, "Links between a stratospheric sudden warming and thermal structures and dynamics in the high-latitude mesosphere, lower thermosphere, and ionosphere," Geophys. Res. Lett. **37**, L13806 (2010). doi 10.1029/2010GL043643
11. H. Liu, E. Doornbos, M. Yamamoto, and S. T. Ram, "Strong thermospheric cooling during the 2009 major stratosphere warming," Geophys. Res. Lett. **38**, L12102 (2011). doi 10.1029/2011GL047898
12. T. Yuan, B. Thurairajah, C.-Y. She, A. Chandran, R. L. Collins, and D. A. Krueger, "Wind and temperature response of midlatitude mesopause region to the 2009 sudden stratospheric warming," J. Geophys. Res. **117**, D09114 (2012). doi 10.1029/2011JD017142
13. L. Sun, W. A. Robinson, and G. Chen, "The predictability of stratospheric warming events: More from the troposphere or the stratosphere?," J. Atmos. Sci. **69** (2), 786–783 (2011). doi 10.1175/JAS-D-11-0144.1
14. J. R. Albers and T. Birner, "Vortex preconditioning due to planetary and gravity waves prior to sudden strato-

spheric warmings," J. Atmos. Sci. **71**, 4028–4054 (2014). doi 10.1175/JAS-D-14-0026.1

15. D. G. Andrews, J. R. Holton, and C. B. Leovy, *Middle Atmosphere Dynamics* (Academic, New York, 1987).
16. O. Buhler, *Waves and Mean Flows* (Cambridge University Press, Cambridge, 2009).
17. J. R. Holton, "The dynamic meteorology of the stratosphere and mesosphere," Meteorol. Monogr. **15** (37), 1–218 (1975).
18. C. McLandress, T. G. Shepherd, S. Polavarapu, and S. Beagly, "Is missing orographic gravity wave drag near 60°S the cause of the stratospheric zonal wind biases in chemistry–climate models?," J. Atmos. Sci. **69**, 802–818 (2012).
19. E. E. Gossard and W. H. Hooke, *Waves in the Atmosphere* (Elsevier, Amsterdam, 1975).
20. C. McLandress, "The seasonal variation of the propagating diurnal tide in the mesosphere and lower thermosphere. Part I: The role of gravity waves and planetary waves," J. Atmos. Sci. **59** (5), 893–906 (2002).
21. N. M. Gavrilov, A. I. Pogorel'tsev, and C. Jakobi, "Numerical modeling of the effect of latitude-inhomogeneous gravity waves on the circulation of the middle atmosphere," Izv., Atmos. Ocean. Phys. **41** (1), 9–18 (2005).
22. D. A. Ortland and M. J. Alexander, "Gravity wave influence on the global structure of the diurnal tide in the mesosphere and lower thermosphere," J. Geophys. Res. **111**, A10S10 (2006). doi 10.1029/2005JA011467
23. S. Watanabe and S. Miyahara, "Quantification of the gravity wave forcing of the migrating diurnal tide in a gravity wave-resolving general circulation model," J. Geophys. Res. **114**, D07110 (2009). doi 10.1029/2008JD011218
24. J. R. Holton, "The generation of mesospheric planetary waves by zonally asymmetric gravity wave breaking," J. Atmos. Sci. **41** (23), 3427–3430 (1984).
25. H. G. Mayr, J. G. Mengel, K. L. Chan, and F. T. Huang, "Middle atmosphere dynamics with gravity wave interactions in the numerical spectral model: Tides and planetary waves," J. Atmos. Sol.-Terr. Phys. **73**, 711–730 (2011).
26. P. Hoffmann, Ch. Jacobi, and C. Borries, "A possible planetary wave coupling between the stratosphere and ionosphere by gravity wave modulation," J. Atmos. Sol.-Terr. Phys. **75–76**, 71–80 (2012). doi 10.1016/j.jastp.2011.07.008
27. N. M. Gavrilov, A. V. Koval', A. I. Pogorel'tsev, and E. N. Savenkova, "Numerical simulation of the response of general circulation of the middle atmosphere to spatial inhomogeneities of orographic waves," Izv., Atmos. Ocean. Phys. **49** (4), 367–374 (2013).
28. N. M. Gavrilov, A. V. Koval, A. I. Pogoreltsev, and E. N. Savenkova, "Numerical modeling influence of inhomogeneous orographic waves on planetary waves in the middle atmosphere," Adv. Space Res. **51** (11), 2145–2154 (2013).
29. A. I. Pogoreltsev, A. A. Vlasov, K. Froehlich, and Ch. Jacobi, "Planetary waves in coupling the lower and upper atmosphere," J. Atmos. Sol.-Terr. Phys. **69**, 2083–2101 (2007). doi 10.1016/j.jastp.2007.05.014
30. M. Inoue, M. Takahashi, and H. Naoe, "Relationship between the stratospheric quasi-biennial oscillation and tropospheric circulation in northern autumn," J. Geophys. Res. **116**, D24115 (2011). doi 10.1029/2011JD016040
31. A. I. Pogoreltsev, E. N. Savenkova, N. N. Pertsev, "Sudden stratospheric warmings: The role of normal atmospheric modes," Geomagn. Aeron. (Engl. Transl.) **52** (3), 357–372 (2014).
32. A. I. Pogoreltsev, "Simulation of planetary waves and their influence on the zonally averaged circulation in the middle atmosphere," Earth Planets Space, **51** (7–8), 773–784 (1999).
33. M. S. Longuet-Higgins, "The eigenfunctions of Laplace's tidal equation over a sphere," Philos. Trans. R. Soc. London **262**, 511–607 (1968).
34. A. I. Pogoreltsev, A. Yu. Kanukhina, E. V. Suvorova, and E. N. Savenkova, "Variability of planetary waves as a signature of possible climatic changes," J. Atmos. Sol.-Terr. Phys. **71**, 1529–1539 (2009). doi 10.1016/j.jastp.2009.05.011
35. N. M. Gavrilov and A. V. Koval, "Parameterization of mesoscale stationary orographic wave forcing for use in numerical models of atmospheric dynamics," Izv., Atmos. Ocean. Phys. **49** (3), 244–251 (2013).
36. J. F. Scinocca and N. A. McFarlane, "The parameterization of drag induced by stratified flow over anisotrophic orography," Q. J. R. Meteorol. Soc. **126** (568), 2353–2393 (2000).
37. Ch. Jacobi, K. Fröhlich, and Y. Portnyagin, "Semi-empirical model of middle atmosphere wind from the ground to the lower thermosphere," Adv. Space Res. **43** (2), 239–246 (2009).
38. I. N. Fedulina, A. I. Pogoreltsev, and G. Vaughan, "Seasonal, interannual and short-term variability of planetary waves in UKMO assimilated fields," Q. J. R. Meteorol. Soc. **130** (602), 2445–2458 (2004).
39. R. E. Dickinson, "Planetary Rossby waves propagating vertically through weak westerly wave guides," J. Atmos. Sci. **25**, 984–1002 (1968).
40. T. Matsuno, "Vertical propagation of stationary planetary waves in the winter Northern Hemisphere," J. Atmos. Sci. **27**, 871–883 (1970).
41. N. M. Gavrilov, A. V. Koval, A. I. Pogoreltsev, and E. N. Savenkova, "Simulating influences of QBO phases and orographic gravity wave forcing on planetary waves in the middle atmosphere," Earth, Planets Space **67,** 86 (2015). doi 10.1186/s40623-015-0259-2
42. D. J. Karoly and B. J. Hoskins, "Three dimensional propagation of planetary waves," J. Meteorol. Soc. Jpn. **60**, 109–123 (1982).
43. J. R. Albers, J. P. McCormack, and T. R. Nathan, "Stratospheric ozone and the morphology of the northern hemisphere planetary waveguide," J. Geophys. Res.: Atmos. **118**, 563–576 (2013). doi 10.1029/2012JD017937
44. J. A. Rice, *Mathematical Statistics and Data Analysis* (Duxbury Press, Pacific Grove, 2006).

Translated by I. Ptashnik